# Life cycle process dependencies of positive-sense RNA viruses suggest strategies for inhibiting productive cellular infection

Harsh Chhajer[a], Vaseef A. Rizvi[b], Rahul Roy[a,c]

[a] Centre for Biosystems Science and Engineering, Indian Institute of Science, Bangalore 560012, India.

[b] Molecular Biophysics Unit, Indian Institute of Science, Bangalore 560012, India.

[c] Department of Chemical Engineering, Indian Institute of Science, Bangalore 560012, India.

## Keywords

Positive sense single stranded RNA virus | Viral intracellular life cycle model | Compartment formation dynamics | Stochastic fate of the infection | Synergy in virus inhibition

**Abstract**

Positive strand (+)RNA viruses are the most common and clinically important human pathogens. Their life cycle processes are broadly conserved across many virus families but they employ different life cycle strategies for their growth in the cell. Upon RNA genome release into the cytoplasm post cellular entry, viral translation generates structural and non-structural proteins that induce intracellular remodelling, forming membrane compartments that foster viral replication leading to virus particle formation. We present a generalized dynamical model for intracellular (+)ssRNA virus growth that accounts for these critical steps. Our model can capture experimental growth dynamics for several RNA viruses as well as parse the effect of viral mutations and host cell permissivity. We show that Poliovirus (PV) employs rapid replication and virus assembly whereas Japanese Encephalitis virus leverages its higher rate of translation and efficient host membrane reorganization for enhanced viral dynamics compared to Hepatitis C virus. Since the slow membrane reorganization represents a crucial bottleneck for replication, stochastic simulations demonstrate that an infection event, even with multiple viral genomes, can go to extinction if all seeding viral RNA degrade before establishing robust viral replication. We estimate this probability of productive cellular infection, termed 'Cellular Infectivity ($\Phi$)' using stochastic simulations. $\Phi$ varies for a virus-host pair with initial virus seeding and life cycle perturbations like increase in cytoplasmic RNA degradation and delay in compartment formation can reduce infectivity. Extent of synergy among these parameters while seemingly diverse for viruses is defined by $\Phi$. Therefore, our model suggests new avenues for inhibition of viral infections by targeting early life cycle bottlenecks.

# Introduction

Positive sense single stranded RNA ((+)ssRNA) viruses from *Enteroviridae* (eg. Poliovirus), *Flaviviridae* (eg. Dengue virus), *Coronaviridae* (eg. SARS) virus families are a major public health challenge. Better understanding of the cellular viral dynamics can help us identify new drug targets and novel antiviral approaches. Virus growth inside the cell is the culmination of a complex interplay of several molecular and cellular processes that has evolved to ensure successful propagation. (+)RNA viruses sequentially translate viral proteins using the positive strand RNA genome upon cell entry, replicate to form nascent genomes from a double stranded RNA (dsRNA) replication intermediate and create new virus particles by encapsidating the (+)RNA genomes with its structural proteins. Members of this class show significant diversity in genome size, physical makeup, constituent viral proteins, host tropism, and chronicity of infection. Yet, they also display striking similarities in cellular life cycle dynamics, largely imitating mechanisms of replication, translation, virus assembly as well as comparable interactions with the host cell machinery. This has motivated the search for universal virus infection features that can be exploited as broad spectrum approaches to inhibit them.

One common characteristic of most (+)RNA viruses is the induction of significant alterations of the intracellular host membrane [1, 2, 3, 4]. The vesicular membranous structures (also known as replication compartments, CMs) formed, provide a conducive micro-environment for efficient viral replication, protect viral RNA and proteins from cytosolic degradation and host defense systems. Impeding membrane re-organizations have been shown to decelerate cellular infection dynamics [5, 6], lower viral yield [7, 8, 9, 10] and reduce the propensity of the virus to establish productive cellular infection in the host cell [6, 11, 12]. In general, failure to establish viral infection has been associated with cellular heterogeneity and is attributed to the random loss of genome segments by RNA degradation in the early stages of infection [13, 14, 15]). This effect manifests at low multiplicity of infection [12] and is common across several virus families. While this suggests that early events in the virus life cycle define the fate of infection, what factors control this mode of viral clearance have not been profiled.

Quantitative measurements and mathematical modeling has tremendously enhanced our understanding of how the subtleties of intracellular processes shape the outcome during viral infections [16, 17, 18, 19, 20, 21, 22, 23, 24] (reviewed in [25]). Understanding derived from these (and combined with their extensions that incorporate extracellular and immune response) have been used to determine effectiveness of interventions and combinations thereof [26, 27, 28, 29, 30]. However, detailed models with explicit molecular details suffer from redundancy in fitting parameters or challenges with estimating parameters experimentally. On the other hand, generalized models fail to accurately emulate the experimentally observed dynamics across a large class of viruses, viral mutations and host cell features. Therefore, there is a need for viral dynamics model that universally capture experimental observations while allowing sufficient inference of molecular mechanisms.

Most viral intracellular viral dynamics models also do not account for the slow formation kinetics of the membranous replication compartments. Since this event coincides with a period sensitive to stochastic fluctuations in viral RNA, it is unclear how membrane reorganisation influences the virus life cycle. In this study, we extend previous models [19, 17, 22] by incorporating the dynamics of replication compartment formation post infection. We show that our model accurately captures several variants of experimentally measured dynamics for Hepatitis C virus (HCV)[22], Japanese Encephalitis virus (JEV) [31] and Poliovirus (PV) [19] infection from literature. Our model highlights differences among virus specific life traits and dynamics and describes observed effects of viral mutations[5] and host cell perturbations [7, 5]. We show that the dynamics of compartment formation is a critical kinetic bottleneck for the viruses. This influences the ability of various viruses to establish a productive infection in the host cell that we refer here as 'cellular infectivity' ($\Phi$). Apart from replication, we recognize limiting formation of CM, increased cytoplasmic degradation of viral RNA and reduced translation as pan-viral strategies, and estimate the synergy among them that can limit cellular infectivity.

# Results

## Cellular viral life cycle model for monopartite (+)RNA viruses

We propose a mathematical model for cellular life cycle of single stranded monopartite (+)RNA viruses, focusing on molecular processes common to such viruses and inspired from previous HCV and PV models [19, 17, 22] (Fig 1a, eq.2, Table 1, details in SI S1). Upon entry into the cell, viral (+)RNA in cytoplasm ($R_{cyt}$) is translated (via host ribosomes) to produce structural ($P_S$) and non-structural ($P_{NS}$) proteins at a rate, $k_t$ (eqs. 2.2, 2.3). Though translation occurs in the cytoplasm, replication is mainly restricted to replication compartments (CMs) [1, 2].

CM formation occurs via extensive alteration to intracellular host membranes [32, 33] induced by viral proteins post infection [1, 2, 3, 34]. Although a slow and critical step conserved across many (+)RNA viral life cycle, previous models did not account for their gradual formation. We model this dynamics using a functional form determined via analysis of ultra-structural characterization data (Fig 1b and Figure S1). Assuming that host homeostasis limits the extent of alterations, we use the popular Weibull function [35] to model the normalized growth of compartments post infection, $f_{CM}$ (eq. 1). $\tau_S$ parameterizes the time scale of the structural manifestation of CMs whereas $n$ defines the steepness of the function. Eq. 1 fits the increase in vesicular membranous structures observed for various (+)RNA viruses [36, 37, 38, 39]. Though the value of $\tau_S$ does not vary significantly, the fits improve as n increases from 2 to 4 suggesting synchrony in CM development (Table S1). $\tau_S$ estimates generally correlate with the timescale of cellular infection across the viruses.

$$f_{CM} = 1 - e^{-(\frac{t}{\tau_S})^n} \tag{1}$$

In context of viral replication, one must consider the ability of these sites to provide protective confinement for RNA replication complex but this aspect has not been quantitatively characterized. Since the structural and functional aspects may be correlated but not identical, we use the same functional form (eq. 1 with n=4), but consider a different maturation time parameter ($\tau_F$) to model the functional maturation of CMs for replication hereon. Although not explicitly incorporated, $\tau_F$ subsumes other delays associated with virus entry and genome un-coating. However, such delays have been shown to be comparably smaller [40, 19, 22].

Celullar homeostasis limits the number of available CMs and hence replication complexes ($R_{cyt}$ and $P_{NS}$) compete for the unoccupied compartments given by $f_{CM} - \frac{RC_{CM}}{N_C}$, where $RC_{CM}$ denotes the number of compartmentalized replication complexes and $N_C$ is the carrying capacity associated with $RC_{CM}$ (Table 1). Therefore, we model the compartmentalization of replication with a logistic function

(eqs. 2.1, 2.4). $RC_{CM}$ synthesize new (+)RNA strands at a rate, $k_r$ (eq. 2.4). The (+)RNA in the compartments ($R_{CM}$) are exported out into the cytoplasm at rate, $k_e$ (eqs. 2.1, 2.5), where it can re-participate in the life cycle. While the viral RNA and proteins degrade in the cytoplasm, we considered minimal degradation in the compartments. Finally, viral assembly occurs in cytoplasm where $R_{cyt}$ associates with $\eta_S$ molecules of $P_S$ to produce extracellular viral particles ($V_T$) at an overall rate of $k_a$ (eqs. 2.3, 2.6).

## Model recapitulates observed HCV life cycle dynamics

Using an iterative approximate Bayesian approach (iABC; see Methods, SI SM1), we fit our life cycle model to the dynamics of intracellular viral RNA, proteins, and extracellular viruses observed and recover parameter estimates for the well characterized HCV infection in Huh7 cells [22] (Fig 1c, Tables 1, S2). We find that new (+)RNA strands are produced at 3.6 $h^{-1}$ ($k_r$) per compartmentalized replication complex ($RC_{CM}$). Using RNA polymerization rate of $150nt/min$ [41], we estimate around three simultaneous replication events per $RC_{CM}$. This is consistent with experimental observations of simultaneous synthesis of multiple viral RNA per replication intermediate (reported to be 5 for the closely related Dengue virus [42]). Similarly, our steady state ratio of viral (+)RNA : (-)RNA (= 54:1) compares well with the experimentally observed ratio of 30:1 [43, 44].

While differences in parameter definition limit exact comparison, we find good agreement with previous efforts to model HCV dynamics. For example, approximating 10 ribosomes [45] translating the viral RNA at a time and $k_t = 23.4h^{-1}$, we predict the HCV protein production rate to be 2.4 $h^{-1}$ per RNA, comparable to prior estimate of the rate limiting step in protein synthesis (polyprotein cleavage rate, 1 $h^{-1}$ [16, 17]). Our estimates for (+)RNA export out of replication compartments is also similar to previous estimates [16]. However, our estimates of virus production is 50-fold faster since the unaccounted delay in CM formation is subsumed in the assembly rate of the existing model [22]. Overall, we recapitulate HCV experimental observations not built a priori into the model as well as match previous estimates for comparable parameters.

To further validate our model, we evaluate the life cycle dynamics of subgenomic HCV (sgHCV) transfected into Huh7 derived (Huh7-Lp and Huh7-Lunet) cells using our model [17] (Figure S2). Our estimates for $k_t$, $k_r$, $N_C$ (carrying capacity of $RC_{CM}$) and $k_c$ (the rate of formation of $RC_{CM}$) for the subgenomic transfection are similar to corresponding estimates for full-genomic infection (Table S2, Table S3) suggesting robustness of our model across different experimental systems for HCV. However, the sgHCV system exhibits delayed RC formation and faster (+)RNA export out of CM likely due to lack of structural proteins, transfection induced cellular artifacts or additional pre-processing of transfected RNA [17]. Interestingly, the highly permissive cell line (Huh7-Lunet) exhibits faster CM formation (1.9 fold lower $\tau_F$) and higher stability of viral dsRNA replication intermediate (11.8 fold larger $N_C$)

compared to Huh7-Lp [46], suggesting efficient replication compartmentalization leads to higher cellular permissivity (Table S3).

## Comparative analysis of monopartite (+)RNA viruses

To understand the differences in life cycle traits among (+)RNA viruses, we further evaluate our model with two distinct class of viruses for which comprehensive viral dynamics data exists, namely *Enterovirus* (PV [19]) and *Flavivirus* (JEV [31]). Comparison of life cycle process parameters (Fig 2, Table S2) shows that the replication rate ($k_r$) and export rate of (+)RNA from compartment ($k_e$) exhibit virus family specific trends (Fig 2c). For example, Poliovirus RNA replicates rapidly (60-fold higher $k_r$) and re-enters the cytoplasmic pool faster (16-fold higher $k_e$) than *Flaviviridae* family (HCV and JEV). Using our estimate of $k_r = 210$ h$^{-1}$ for PV (similar to 133 h$^{-1}$ reported earlier [19]) and assuming PV genome replication takes 100 secs [47], we predict 5.8 simultaneous replication events occur per $RC_{CM}$ closely matching previously measured values of 6.5-7 [48, 49]. On the other hand, JEV displays ≈3 simultaneous replications per $RC_{CM}$ (assuming RNA elongation rate of $150nt/min$ [41]) comparable to HCV and Dengue as discussed above. This further shows that our model captures the now well recognized fact that CMs are sites of multiple parallel replication reactions without explicitly assuming it [2].

Protein synthesis rate, $k_t = 18.9h^{-1}$ for PV is comparable to HCV and similar to previous report [19] but JEV proteins are produced five times faster. Although polyprotein processing and host cell features affect $k_t$, we attribute the high $k_t$ values for JEV to its RNA cap dependent translation initiation [50] compared to the IRES mediated mechanism employed by HCV and PV [50, 51]. Faster protein production and an associated early induction of membrane re-organization could be responsible for the faster functional maturation of CM for JEV.

Virus assembly and generation defined by $k_a$ is significantly ($> 10^5$ fold) faster for PV compared to the *Flaviviridae* viruses (HCV and JEV) reflecting their corresponding complexity in assembly and maturation. While the detailed mechanisms of virus assembly remains poorly understood, HCV and JEV are enveloped viruses made of 180 copies of three different structural proteins [52, 53] that require maturation post assembly whereas PV is a smaller non-enveloped virus [54].

These differences in life cycle traits are robust to alternative formulations for replication compartment formation (SI S5) whether we consider pre-formed CM ($f_{CM} = 1$), or a more gradual rise in compartments (Weibull exponent, n = 2). Similarly, stoichiometry of $P_{NS}$ in formation of $RC_{CM}$, or consideration of replication coupled assembly of viral particles [22] does not alter our virus specific parameter trends. While goodness of fit based on cumulative AIC values for the three viruses (Table S4) demonstrates a marginal advantage in favour of our main model, measured CM formation dynamics [32, 33] support our choice of the model. Moreover, independent experimental corroborations like recovery of steady state levels of replication intermediate [55, 17, 56] and steady state positive/negative RNA ratios [44, 43],

(Table S4) further supports our model. Due to the lack of molecular details for virus assembly, our model only qualitatively captures the virus assembly and release dynamics and we cannot discriminate between alternate sites (CMs vs cytoplasm) for virus assembly.

## Conserved and virus-specific determinants shaping viral life cycle

To evaluate how perturbations in life cycle model parameters affects the viral dynamics, we employed temporal sensitivity analysis (TSA) using the eFAST algorithm ([57]) and examined parameters critical to the life cycle. TSA profiles of $RC_{CM}$, the key intermediate and a surrogate for viral replication, highlights three distinct dynamical regimes for the viruses (Fig 3 a). The initial establishment (E) phase is sensitive to the delay in formation of CM ($\tau_F$), and displays minimal replication due to shortage of CM. The next growth (G) phase represents the rapid increase in viral RNA production and is influenced by parameters governing the increase of (+)RNA in the cytoplasm. Growth phase is sensitive to changes in viral replication rate ($k_r$), the kinetics of (+)RNA export from CM ($k_e$) and the rate of cytosolic degradation of (+)RNA ($\mu_R$) that determine the formation of dsRNA (replication intermediate). The final saturation (S) phase is defined by the pseudo-steady state behaviour primarily regulated by the carrying capacity for $RC_{CM}$ ($N_C$). Though the TSA trends are qualitatively similar, the time associated with each phase varies with the virus. The length of the E phase correlates with the estimate for $\tau_F$, and time span of growth phase reflects the estimates for $k_r^{-1}$ and $k_e^{-1}$. So, while the G phase is comparable for HCV and JEV, it is very short for PV as is evident with the rapid increase in PV RNA in a short window of 2 h [19].

Differences in the TSA profiles across the viruses are more evident when $V_T$ (Fig 3b) and $R_{cyt}$ are considered (Figure S9). The profiles associated with $V_T$ are particularly informative in identifying 'choke points' and their effectiveness for different viruses. We postulate that perturbations to replication ($k_r$) would be more effective than translation ($k_t$) against JEV but vice versa for inhibiting Poliovirus growth. For HCV, viral dynamics is influenced by viral RNA degradation ($\mu_R$) to a large extent followed by translation and replication. $\mu_R$ is critical for HCV life cycle as its (+)RNA has a large dwell time in the cytoplasm (due to its large $\tau_F$, $k_t^{-1}$ and $k_c^{-1}$). This shows how model parameter sensitivity can generate virus-specific insights into life cycle intervention strategies.

## Changes in $N_C$ and $\tau_F$ mimic the effect of perturbations to compartment formation

Among the critical parameters, $\tau_F$, $k_e$ and $N_C$ that are defined by the CM formation dynamics and its architecture. Various viral [1, 2, 4, 34, 58] and host perturbations [59, 60, 61, 62] and drug interventions [9, 8, 10] have been reported to alter membrane reorganisation, which ultimately affects infection kinetics as well as the steady state achieved in the later stages. To test how the dynamics of CM generation

defines the virus life cycle, we emulate some of these perturbations by varying $\tau_F$ (for kinetics) and $N_C$ (for steady state) and compare it to experimental observations.

Reticulon 3 (RTN3) is an Endoplasmic Reticulum (ER) shaping host protein shown to be involved in ER membrane re-organization during various (+)RNA viral infections [59, 60]. Silencing RTN3 in host cells reduces viral replication of Flaviviruses [7] and Enteroviruses [6], but increases it in case of HCV [5]. In our model, $N_C$ is the sole parameter that affects the steady state levels of viral (-)RNA levels ($RC_{CM}$), which is perturbed upon RTN3 silencing in host cells [7]. By just varying $N_C$, we are able to reproduce correlated fold changes in (-)RNA levels, viral titre and $P_{NS}$ with respect to viral RNA as observed for various Flaviviruses[7] and HCV[5] upon silencing RTN3 in host cells (Fig. 3c-inset, c, d). This also suggests that the steady state level correlations among the various virus constituents are appropriately accounted in our model.

Our steady state level estimates for virus and protein levels with viral (+)RNA are distinct for the three viruses considered here. For HCV and PV, $P_{NS}$ vary linearly with viral (+)RNA level, however it is sub-linear in case of JEV (Fig. 3d). The increase in $V_T$ with viral (+)RNA levels is super-linear and sub-quadratic, for JEV and HCV, respectively whereas it is linear for PV (Fig. 3d). The trends are corroborated by steady state analysis of the model (refer SI S3). Efficient assembly for PV ($k_a R_{cyt} >> \mu_P$) leads to $R_{cyt}$-independent level of $P_S$ ($P_S \approx \frac{k_t}{\eta_S k_a}$), resulting in linear relation between $V_T$ and (+)RNA ($V_T \approx \frac{k_r N_C}{\mu_R} \approx \frac{R_{cyt} k_t}{\mu_R \eta_S}$). The analysis also suggests that when comparing HCV and JEV, higher $k_t.k_a$ estimate contributes to faster assembly of $R_{cyt}$. Thus $R_{cyt}$ (and consequently $P_{NS} = \frac{k_t R_{cyt}}{\mu_P}$) increases sub-linearly with increase in $N_C$ for JEV.

To evaluate the effect of the compartment formation kinetics on the viral dynamics, we compare various NS4B mutants shown to be defective in inducing membrane re-organization [34, 58]. Using $\tau_F$ as the fitting parameter (details in SI SM3), the model is able to accurately recapitulate the normalized protein dynamics observed for these sgHCV mutants [5] (Fig 3e). The estimated $\tau_F$ for the NS4B sgHCV mutants R52D, Y63A and R52DY63A, are 63, 101 and 80 h respectively compared to 5.8 h for the WT virus highlighting how increased delay in CM formation affects viral dynamics.

## Compartmentalization of replication defines the fate of virus infection

Compartmentalization of viral replication establishes a site of efficient (+)RNA replication, protected from cytoplasmic degradation in the infected cell. However, compartmentalization is not always guaranteed upon virus entry, with the possibility of degradation of viral genome in the host cytoplasm before membrane reorganization. We posit that the infection outcome of viral seeding event is an all-or-none phenomena that is determined at the onset of the infection by the opposing effects of cytoplasmic viral RNA degradation and the formation of $RC_{CM}$ (Fig. 4a). Indeed, stochastic simulations of the HCV life cycle demonstrates these two outcomes (Fig. 4b). All realizations where $RC_{CM}$ is formed before the

complete degradation of viral RNA result in a productive infection, otherwise the infection extinguishes. We define this likelihood of productive infection establishment post virus seeding as 'cellular infectivity', $\Phi$.

$\Phi$ ranges between zero (deterministic extinction of infection) and one (deterministic establishment of productive infection) depending on viral seeding load (N) and virus-host factors that are critical in the early stages of virus life cycle. $\Phi$ increases monotonically till saturation with N (Fig 4c). It is also modulated by the kinetics of viral processes leading to compartmentalization of replication ($k_t$, $\tau_F^{-1}$, $k_c$) and the stability of viral genome in host cytoplasm ($\mu_R^{-1}$) [Fig 4d, Figure S10, Figure S11]. This is consistent with reports that show reduction in success rate of infections due to host cell perturbation [11] or for viral mutants [6], where CM formation is hindered. This effect is also associated with the antiviral activity of membrane re-organization inhibitors like K22 [9, 8] that likely influences $\tau_F$. $\Phi$ also increases from HCV to PV to JEV based on our estimates of the life cycle parameters above (Fig 4c). We estimate that rate of non-productive, single virus JEV and HCV infections are 40% and 85% respectively (Fig. 4c). At larger viral seeding of N=8, $\Phi$ for HCV is 0.95, closely matching the 95.28% infection success rate observed due to an infection with 8 genomes per cell (measured inside the cell at 3 hpi [22]).

Interestingly, while success rate of 10 seeding genomes remains unaffected when $\tau_F$ is increased (by 2-fold), the success rate drops by 47% upon identical change in $\tau_F$ for single genome infection. This mirrors the higher reduction in fraction of productive PV infected cells observed due to action of membrane re-organization inhibitor, PIK93 [63] at low multiplicity of infection [12]. This effect also contributes to the synergy observed between entry inhibitors (effectively decreasing N) and other antiviral agents, like protease inhibitors, membrane re-organization inhibitors, cyclophilin inhibitors, against HCV [64, 65]. The effects of these inhibitors on model parameters are summarized in Table S5.

## Synergy among strategies reducing cellular infectivity

Since the life cycle parameters that limit $\Phi$ collaborate in complex ways, we further characterized the synergy ($\Psi$) among them. We use the Bliss independence criterion [66] to evaluate this synergy since these life cycle events occur independently at the molecular level. Apart from reducing $\Phi$ independently, $\tau_F$ and $\mu_R$ positively synergize when combined ($\Psi_{\tau_F,\mu_R} > 1$) for the viruses (Figs. 5a, Figure S12a,b). For example, simultaneous doubling of both $\tau_F$ and $\mu_R$ resulted in an eight fold reduction in $\Phi$ compared to the product of their independent actions in case of HCV. In our formalism, synergy stems from enhanced delays in the formation of compartments leading to increased exposure of viral RNA to cytosolic degradation. By extension, other RNA viruses that employ compartmentalization to stabilize replication will also display such character.

At first glance, the quantitative relationship for $\tau_F - \mu_R$ synergy varies with the virus-host system and seeding density, in addition to intensity of perturbations in a complicated fashion (Figs. 5b). Under

conditions where $\Phi \to 1$ or is close to extinction of infection ($\Phi \to 0$), perturbations do not influence $\Phi$, individually or in combination. But, we observe high synergy when $\Phi$ is farther from these two extreme outcomes. Figure 5c shows that $\Psi_{\tau_F,\mu_R}$ decreases with $\{(1-p_0)+p_{12}\}$, a surrogate for how far the system is from either of the two deterministic limits where $p_0$ and $p_{12}$ denote $\Phi$ in unperturbed and doubly perturbed conditions, respectively (SI S4). Similar synergy and associated negative correlation with $\{(1-p_0)+p_{12}\}$ is also predicted for $\tau_F - k_t$ (Figure S12c-g). Therefore, interventions that target membrane reorganization can be combined with other antiviral inhibitors to target early life cycle events in order to achieve effective viral clearance.

# Discussion

We incorporated the dynamics of replication compartment (CM) formation accompanying cellular infection into a simplified intracellular life cycle description for monopartite (+)RNA viruses. This allowed us to capture observed dynamics for viruses spanning multiple (+)RNA virus families, parse diverse effects of host cell susceptibility, virus mutations and external interventions, and identify stochasticity associated with establishment of (+)RNA infection upon cell entry.

Based on temporal dependencies among model parameters, the viral life cycle can be categorized into three phases - establishment, growth and saturation (steady state). High translation efficiency (5'cap-dependent ribosome loading and fast CM formation (linked to faster protein production), as observed for Japanese Encephalitis virus (JEV), results in a rapid completion of the establishment phase. Following the compartmentalization of replication, the life cycle enters the growth phase that is marked by positive feedback from the nascent RNA in the CM fueling the replication process. Kinetics of replication ($k_r$), (+)RNA export from CM ($k_e$) and (+)RNA degradation in cytoplasm shapes this phase, which is particularly short for PV, owing to its rapid replication and export. Virus generation ($k_a$) for PV is also very fast compared of the *Flaviviridae* members, which we attribute to differences in virus structural complexity, assembly and egress mechanisms [67, 68]. Replicative fitness (defined by $k_r$ and $N_C$) and viral RNA stability ($\mu_R^{-1}$) determines the steady state levels of cytoplasmic (+)RNA and viral titre in the final saturation phase for all viruses. Not surprisingly, $k_r$, which is targeted via nucleoside inhibitors, remains a promising pan-viral drug target. Additionally, temporal sensitivity profiles suggests that the replication kinetics for JEV, is more sensitive to perturbations compared to translation whereas the reverse is true for PV. Virus production seem to be robust against perturbation to assembly rate ($k_a$) for all the three viruses. Coupled with steady state analysis, this suggests that genomes are packaged more efficiently than they are degraded.

In our formalism, we also find dynamics of CM formation (broadly captured by $\tau_F$ and $k_c$) to be a key kinetic barrier in the early stage of the (+)RNA virus life cycle and it has been aptly described as the 'load and choke point' [17]. We demonstrate that ability of viruses to successfully establish infection in the host cell is stochastic and 'cellular infectivity' ($\Phi$) is determined at the onset of the infection. Such early stochastic extinction of viral infection has been similarly suggested due to biological noise [14, 13]. For synchronous co-infection, we predict that multi-hit infections are more likely to result in productive infection than single hit infection (as observed for PV [69]).

In a cell population, $\Phi$ quantifies the fraction of cells successfully infected upon entry of infectious viral particle(s) and correlates with the multiplicity of infection (MOI). As with MOI (discussed in [68]), we see that $\Phi$ also depends on seeding density (N) and virus-host determinants. Factors like viral genome stability in cytoplasm ($\mu_R^{-1}$) and kinetics of viral processes antecedent to formation of $RC_{CM}$ affects productive infection. Infectivity is highly sensitive to $\tau_F$ (compared to $k_t$ or $k_c$). This could explain the

reduction in $\Phi$ observed when membrane re-organization is hindered either due to viral mutations [6] or host cell perturbations [11]. Similarly, we speculate that the infectivity of a virus in a host cell could also determine the permissiveness of the host cell line [17, 70, 71].

Some of the early-infection parameters can also control cellular infectivity more effectively in combination, displaying higher order effects due to their mutual action on common viral entities or processes. Our predictions are consistent with increased antiviral activity observed for membrane re-organizing inhibitor at lower MOI [12] as well as synergy observed between entry inhibitors (that reduce N) and several classes of antiviral agents against HCV [64, 65]. Thus interventions delaying CM formation, slowing translation, increasing viral degradation and reducing viral seeding, are expected to synergize to reduce infectivity. Further, when viral and cellular heterogeneity is considered, such synergism would further accentuate this all-or-none dimorphism [15, 13].

Decrease in overall viral production due to lower infectivity can reduce viral seeding for the subsequent round of infections. Due to its dependency on viral seeding, such reduction in infectivity will manifest in a compounding effect that reduces the effective basic reproduction number, $R_0$ and leads to viral clearance. Therefore, cellular antiviral strategies that target cellular infectivity can be used in conjunction with other interventions (including innate immune response) that decrease the virus load.

Overall, our general theoretical framework can serve as a starting point for analysis of novel viruses with limited characterization, to generate insights into life cycle traits and bottlenecks, motivate design of experimental studies for insightful investigation and evaluate antiviral strategies.

# Methods

## Experimental data and data fitting

All experimental data sets used were curated from literature. Data for estimation of $\tau_S$ (using eq. 1) was taken from [36, 37, 38, 39]. Cellular life cycle dynamics for HCV, JEV and PV were obtained from [22], [31] and [19], respectively. JFH1 (sgHCV strain) transfection dynamics and polyprotein dynamics of HCV NS4B mutants was obtained from [17] and [5], respectively. Effect of RTN silencing on viral dynamics were curated from [5, 7]. Figure digitization and data extraction were done using WebPlotDigitizer (Ankit Rohatgi, WebPlotDigitizer).

Estimation of parameter values was done using Iterative Approximate Bayesian computation (iABC) algorithm ([72, 19], SI SM1), which iteratively improves upon the distribution of parameter values based on $\chi^2$ statistics computed between model prediction and observed data, $\chi^2 = \sum \frac{(Prediction-Data)^2}{Var(Data)}$. In case variance for experimental data was not reported, we assumed a 10% relative error in the reported data and variance used is explicitly shown in the figures. Practical identifiability is defined as the pairwise correlation in values of parameter combinations derived from the final iteration of estimation [19]. Further details are provided in the SI Methods.

## Model analyses: Temporal sensitivity analysis and calculating $\Phi$ and $\Psi$

We used extended Fourier Amplitude Sensitivity Test (eFAST) [57, 73], to estimate the corresponding temporal sensitivity profile. Sensitivity indices for $RC_{CM}$, $V_T$ and $R_{cyt}$ were evaluated every 15 minutes through the course of the infection to get the temporal profile.

To estimate cellular infectivity ($\Phi$), stochastic realizations of the life cycle were implemented using the Gillespie algorithm [74], and classified as (a) successful infection ($I_S$): if $RC_{CM}$ is formed, (b) failed infection ($I_F$): if all viral (+)RNA degrade, and (c) inconclusive: neither happen till 12 h. The fate of infection was decided in all stochastic realizations for HCV life cycle (slowest of the three viruses) by 12 h. We consider only the 'conclusive' realizations and define $\Phi$ as $\frac{\#(I_S)}{(\#(I_S)+\#(I_F))}$. Dynamics of $f_{CM}$ is incorporated by updating it at every event or at steps of $\frac{\tau_F}{20}$, whichever is shorter. This limits the error due to discretization of $f_{CM}$ to 6.5%.

To calculate (Bliss) synergy, $\Psi$, between two parameters, $a_1$ and $a_2$, to reduce $\Phi$ we define $p_0$, $p_1$, $p_2$ and $p_{12}$ as $\Phi$ corresponding to no perturbation, perturbation in parameter $a_1$, perturbation in parameter $a_2$, and simultaneous perturbations in parameter $a_1$ and $a_2$, respectively. $g_X$ denotes $\frac{p_X}{p_0}$ for $X \in 1, 2, 12$. Synergy in perturbations to reduce $\Phi$ is given by, $\Psi = \frac{g_1.g_2}{g_{12}}$ (Bliss criterion [66]). Here, if $\Psi > 1$, that is, $g_1.g_2 > g_{12}$, then individual perturbations independently are not able to reduce $\Phi$ as effectively as combined effect of the two.

# Acknowledgement

This work was supported by the Indian Institute of Science Bangalore (RR), Wellcome Trust—DBT India Alliance intermediate fellowship (RR), Council of Scientific and Industrial Research fellowship (VR) and the Prime Minister Research Fellowship (HC). We thank Narendra Dixit, Mohit Jolly, Sunaina Banerjee and Suraj Jagtap for valuable feedback on the manuscript.

Table 1: **Life cycle Model Parameters**

| Parameter [Units] | Description | HCV in Huh7 | JEV in PS | PV in HeLaS3 |
|---|---|---|---|---|
| **Free parameters** * | | | | |
| $\tau_F$ [h] | Time constant for functional development of CMs | 5.8 | 2.6 | 4.2 |
| $k_t$ [h$^{-1}$] | Protein production rate per $R_{cyt}$ | 23.7 | $1.6\times10^{2}$ | 18.9 |
| $k_c$ [molecules$^{-1}$.h$^{-1}$] | Formation rate of $RC_{CM}$ by association of $R_{cyt}$, $P_{NS}$ & unoccupied compartments | $2.6\times10^{-3}$ | $1.6\times10^{-2}$ | $1.2\times10^{-2}$ |
| $k_r$ [h$^{-1}$] | (+)RNA synthesis rate per $RC_{CM}$ | 3.6 | 3.7 | $2.2\times10^{2}$ |
| $k_e$ [h$^{-1}$] | Export rate of $R_{CM}$ into the cytoplasm | $6.6\times10^{-2}$ | $7.2\times10^{-2}$ | 1.1 |
| $N_C$ [number] | Carrying capacity of $RC_{CM}$ in host cell | $8.8\times10^{1}$ | $1.21\times10^{3}$ | $1.62\times10^{3}$ |
| $k_a$ [molecules$^{-1}$.h$^{-1}$] | Effective virus generation rate | $3.6\times10^{-8}$ | $8\times10^{-9}$ | $5.6\times10^{-3}$ |
| **Fixed parameters** # | | | | |
| $\eta_S$ | Number of capsids per virus particle | 180 | 180 | 60 |
| $\mu_R$ [h$^{-1}$] | Degradation rate of $R_{cyt}$ | 0.25 | 0.25 | 0.25 |
| $\mu_P$ [h$^{-1}$] | Degradation rate of $P_S$ and $P_{NS}$ | 0.11 | 0.11 | 0.11 |
| $\mu_V$ [h$^{-1}$] | Degradation rate of $V_T$ | $6\times10^{-3}$ | $6\times10^{-3}$ | $6\times10^{-3}$ |

* Values reported here indicate the median of the distribution estimated from data fitting (Fig. 2c).
# Values used for fixed parameters were obtained from literature [53, 52, 54, 22] or by analysing reported observations [22], as indicated in SI text S9.

**Cellular life cycle model**

$$\frac{dR_{cyt}}{dt} = k_e.R_{CM} - k_a.P_S.R_{cyt} - \mu_R.R_{cyt} - k_c.P_{NS}.R_{cyt}.(f_{CM} - \frac{RC_{CM}}{N_C}) \tag{2.1}$$

$$\frac{dP_{NS}}{dt} = k_t.R_{cyt} - \mu_P.P_{NS} - k_c.P_{NS}.R_{cyt}.(f_{CM} - \frac{RC_{CM}}{N_C}) \tag{2.2}$$

$$\frac{dP_S}{dt} = k_t.R_{cyt} - \eta_S.k_a.P_S.R_{cyt} - \mu_P.P_S \tag{2.3}$$

$$\frac{dRC_{CM}}{dt} = k_c.P_{NS}.R_{cyt}.(f_{CM} - \frac{RC_{CM}}{N_C}) \tag{2.4}$$

$$\frac{dR_{CM}}{dt} = k_r.RC_{CM} - k_e.R_{CM} \tag{2.5}$$

$$\frac{dV_T}{dt} = k_a.P_S.R_{cyt} - \mu_V.V_T \tag{2.6}$$

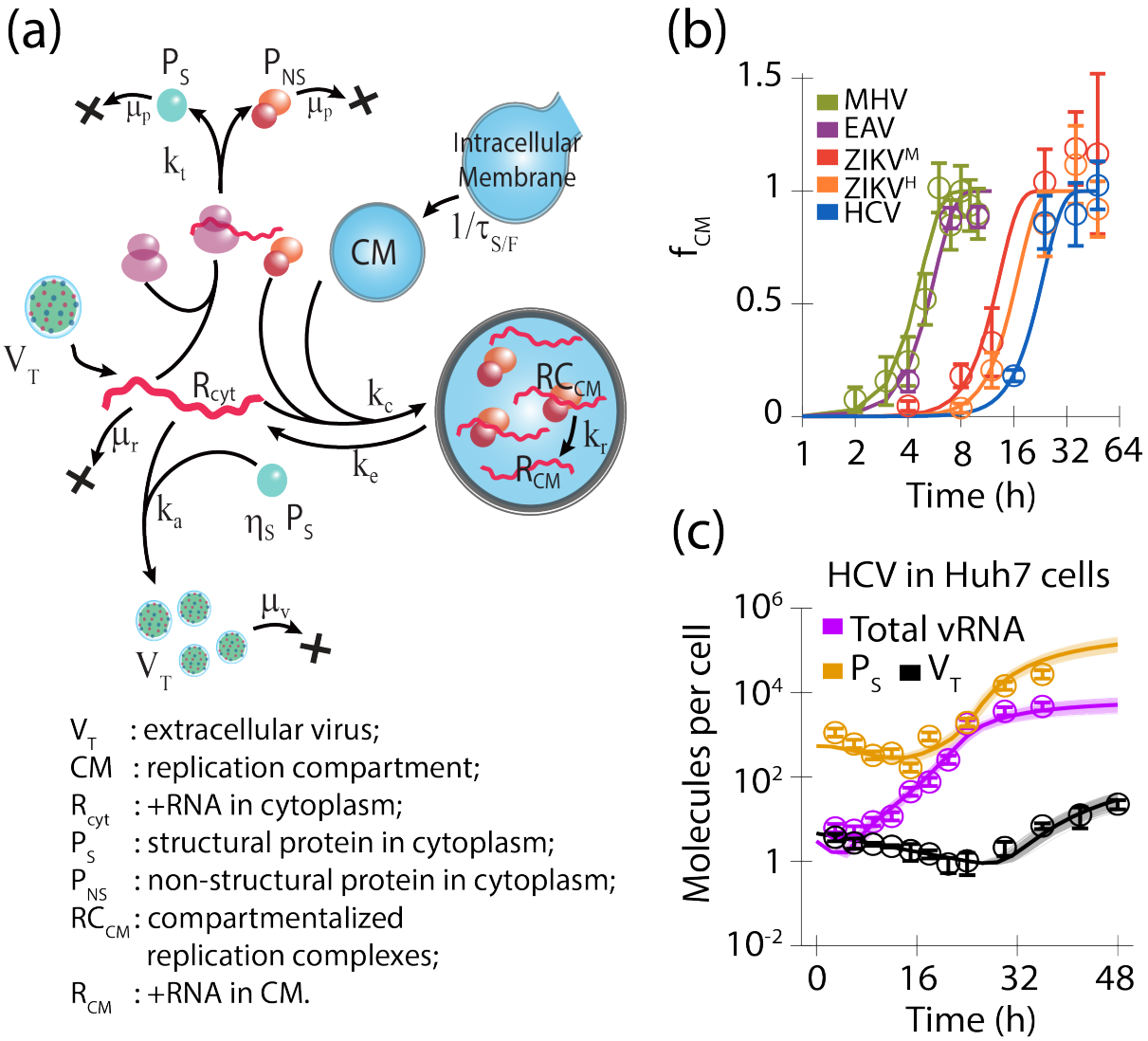


Figure 1: **Incorporating compartment formation dynamics in viral life cycle model**
(a) Schematic of the viral life cycle model: In the cytoplasm, the (+)RNA ($R_{cyt}$) is translated by the host ribosomes to produce viral structural ($P_S$) and non-structural proteins ($P_{NS}$). $\eta_S$ copies of $P_S$ associates with $R_{cyt}$ to assemble virus particles ($V_T$). During (+)RNA viral infection, the host intracellular membrane is re-organized to form compartments (CM) which harbours viral replication complex. These compartmentalized complexes ($RC_{CM}$) are actively replicated to produce new (+)RNA strands, which are exported out into the cytoplasm to fuel translation, replication or assembly.
(b) Fitting normalized dynamics of compartment formation ($f_{CM}$) observed for different (+)RNA viruses using eq. 1 (with n = 4). ZIKV$^M$ and ZIKV$^H$ denotes the MR766 and H/PF/2013 strains of Zika virus respectively. Data: [36, 37, 38, 39]
(c) Model fit for observed cellular life cycle dynamics of HCV infection in Huh7 cells [22].
In (b) and (c), hollow circles and error bars correspond to data used for fitting, whereas similarly colored lines represent model fitting. Thin lines denote dynamics predicted using each of the best parameter combinations identified in the final iteration of iABC (see Methods, and S6 and S8 in SI). Thick lines indicates average of these simulations.

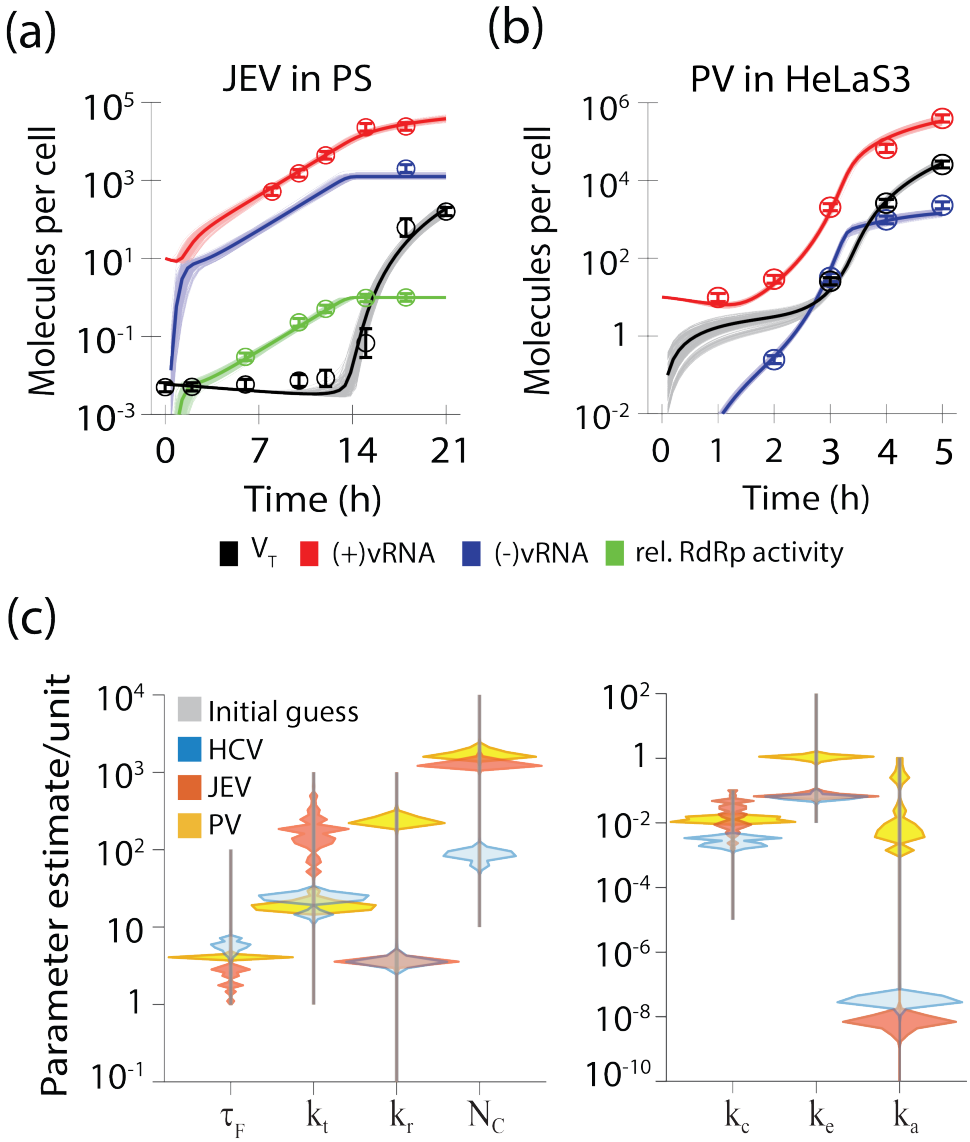


Figure 2: **Comparison of monopartite (+)RNA viruses**
Model Fits (thin lines, best parameter fits; thick line, average of best fits) for the observed cellular life cycle dynamics of (a) JEV infection in PS cells [31], and (b) PV infection in HeLaS3 cells [19]. (c) Comparing of parameter value estimated for HCV, JEV and PV life cycle dynamics

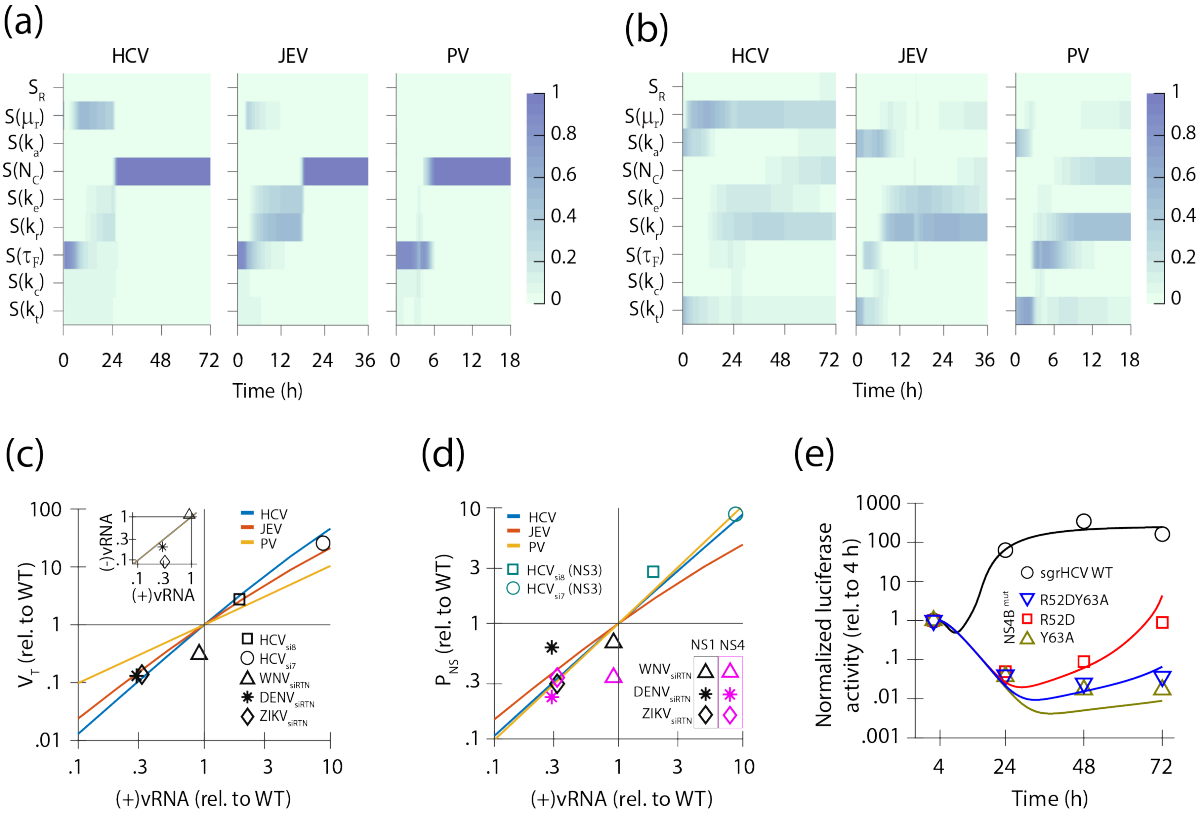


Figure 3: **Perturbation analysis of viral life cycle parameters**
Parameter-temporal sensitivity profiles for dynamics of (a) $RC_{CM}$ and (b) $V_T$, for HCV, JEV and PV are shown. Here $S(X)$ denote the profile associated with parameter, X, and $S_R = S(\mu_P) + S(\mu_V) + S(dummy)$. Time axis is not to scale across profiles for different viruses. Model estimated fold change in steady state levels (c) $V_T$ vs (+)RNA, (d) $P_S$ vs (+)RNA and (c-inset) (-)RNA vs (+)RNA, due to perturbation in $N_C$ is compared to various results from experimentally induced perturbations in RTN3 protein. Solid lines are model predictions and symbols represent experimental data. Marker shape and color differentiate viruses and protein (measured) respectively. (e) Prediction for viral protein dynamics for NS4B mutants (defective in inducing membrane remodelling) of sgHCV is fit by varying only $\tau_F$. Solid lines and symbols show best fit predictions and data, respectively.

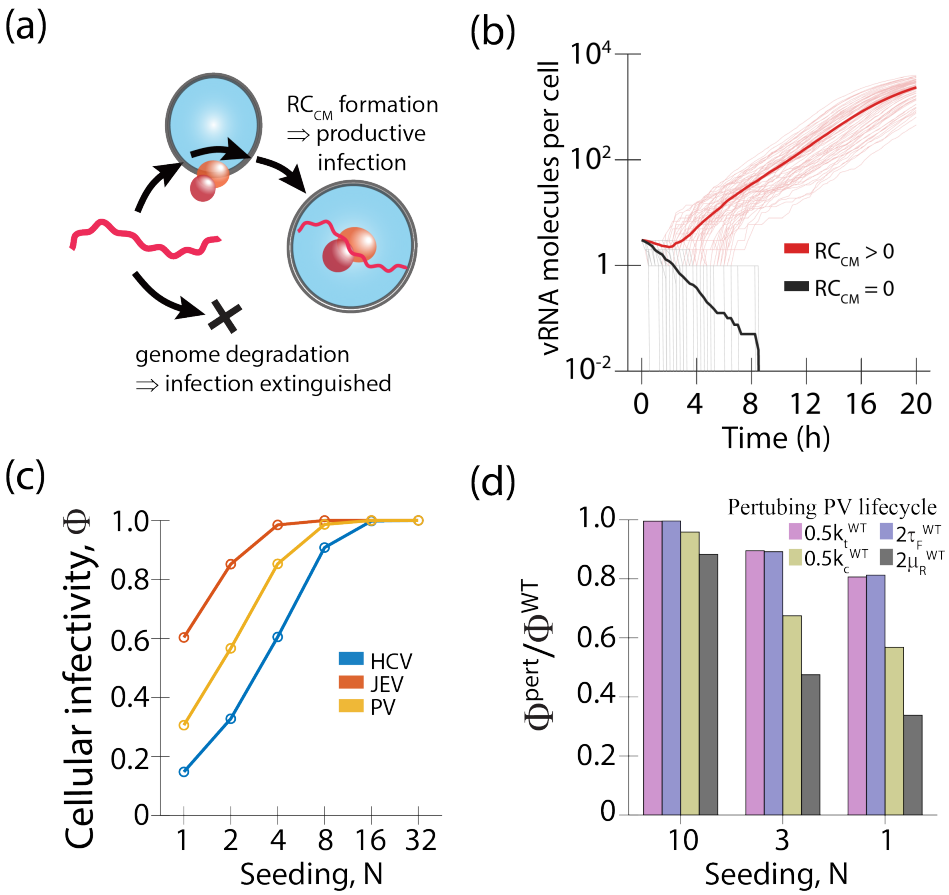


Figure 4: **Stochastic fate of productive viral infection**
(a) Compartmentalization of replication ($RC_{CM}$ formation) is required to sustain intracellular (+)RNA viral infection. Early in the infection, as the cytoplasmic viral RNA is encapsulated in vesicular compartments, high replication rate and minimal degradation leads to productive infection. Early degradation of all viral RNA in the cytoplasm leads to complete extinction of infection. (b) Stochastic realizations of cellular life cycle dynamics of HCV in Huh7 cells at viral seeding of 3. Thin lines indicate dynamics of simulated realizations when at least 1 $RC_{CM}$ (red) was formed and when no $RC_{CM}$ (black) were formed respectively; thick lines represent corresponding averages. (c) Probability of establishment of infection ($\Phi$) as a function of seeding number (N) for HCV, JEV and PV is shown. (d) Fold change in $\Phi$ (for PV) with varying N for different parameters is shown. $k_t^{WT}$, $k_c^{WT}$ and $\tau_F^{WT}$ correspond to estimates for PV (Table S2), and $\mu_R^{WT} = 0.25$ h$^{-1}$.

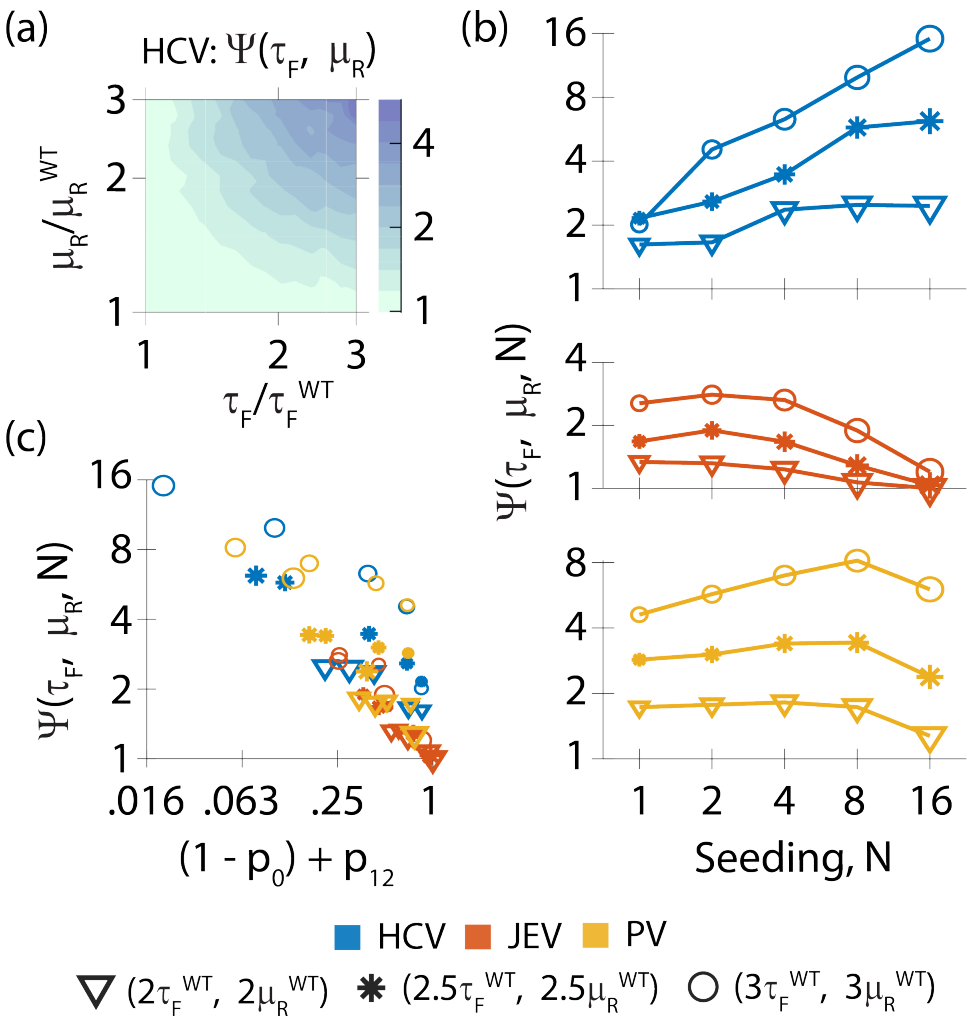


Figure 5: **Interaction between strategies reducing infectivity**
(a) $\Psi(\tau_F, \mu_R)$ evaluates the synergy between $\tau_F$ and $\mu_R$ to reduce $\Phi$ (according to Bliss synergy [66]), for HCV at seeding, N = 3. $\Psi > 1$ indicates a positive synergy in reduction of $\Phi$. (b) Variation of $\Psi(\tau_F, \mu_R)$ for different perturbation strengths (denoted by different markers) with viral seeding (N) for HCV (blue), JEV (red) and PV (yellow). (c) $\Psi(\tau_F, \mu_R)$ shows a negative correlation with $\{(1-p_0)+p_{12}\}$, which increases as it approaches either the limit of 'deterministic sustenance ($p_{12} \to 1$)' or 'deterministic extinction ($p_0 \to 0$)'. Here $\tau_F^{WT}$ corresponds to corresponding estimate for the virus and $\mu_R^{WT} = 0.25$ $h^{-1}$. Marker properties are consistent in (b) and (c) and larger markers correspond to higher N.

# Supplementary Information

## SI S1 Description of model formulation

## SI S2 Revisiting the assumptions

## SI S3 Steady state analysis

## SI S4 Quantifying "far from determinstic regime"

## SI S5 Alternate models

## SI SM1 Iterative Approximate Bayesian computation (iABC) for parameter estimation

## SI SM2 Practical Identifiability calculation

## SI SM3 Implementation details

**Figure S1 Compartment formation dynamics:** Fitting observed dynamics of compartment formation with (a) n = 2, (b) n = 3 and (c) n = 5. Data: [36, 37, 38, 39]. ZIKV$^M$ and ZIKV$^H$ denotes the MR766 and H/PF/2013 strains of Zika virus respectively. In each case the fitting and/or distribution correspond to that estimated in the fifth iteration of iABC. Here hollow circles and error bars correspond to data used for fitting, whereas similarly colored lines represent model fitting. Thin lines denote dynamics predicted using each of the best parameter combinations identified in the final iteration of iABC (see Text S6 ans S8). Thick lines indicates average of these simulations.

**Figure S2 Parsing effects of host cell permissiveness** Fitting life cycle model ($M_4^1$, eq. 2) to transfection dynamics of sgHCV (JFH1 strain) in (a) low permissive (Huh7-Lp) and (b) high permissive (Huh7-Lunet) cell lines. Initial condition used in both cases: $R_{cyt} = 100$. We consider constant relative error in observation. We ignore viral assembly ($k_a = 0$) for JFH1 strain. Data source: [17]. (c) Comparing distribution of parameter estimated for the two cases (grey: Huh7-Lp; red: Huh7-Lunet). Pairwise correlation in the values of parameters estimated for transfection in (d) Huh7-Lp and (e) Huh7-Lunet cell. Here the fit and parameter estimates correspond to that estimated in the third iteration of iABC. In (a) and (b), hollow circles and error bars correspond to data used for fitting, whereas similarly colored lines represent model fitting. Thin lines denote dynamics predicted using each of the best parameter combinations identified in the final iteration of iABC (see SI.Methods). Thick lines indicates average of these simulations.

**Figure S3 Fitting transfection dynamics using different fitting options** Comparing distribution of parameter estimated for the two cases (grey: Huh7-Lp; red: Huh7-Lunet) (a) using initial condition $R_{cyt} = 10$ and considering error in observation as reported in the publication[17], (b) using initial condition $R_{cyt} = 1000$ and considering constant relative error in observation. Data source: [17]. Here the parameter estimates correspond to that estimated in the third iteration of iABC.

**Figure S4 Algorithm convergence and practical identifiability analysis for fitting cellular dynamics of HCV, JEV and PV using $\mathbf{M}_4^1$** Variation of minimum (red) and maximum (blue) $\chi^2$, corresponding to parameter combinations selected, with each progressive iteration of iABC while fitting life cycle dynamics of (a) HCV, (b) JEV and (c) PV. Pairwise correlation (see SI SM2) in the values of parameters estimated (in the eighth iteration of iABC) for (d) HCV, (e) JEV and (f) PV.

**Figure S5 Alternate model, $\mathbf{M}'$: $f_{CM}$ formulation variant where $f_{CM} = 1$** Fitting model to observed dynamics of (a) HCV, (b) JEV and (c) PV. Data source: [22, 31, 19] (d) Comparing distribution of parameter estimated for the three viruses: HCV (blue), JEV (orange) and PV (yellow). Here the fit and parameter estimates correspond to that estimated in the eighth iteration of iABC. In (a), (b) and (c), hollow circles and error bars correspond to data used for fitting, whereas similarly colored lines represent model fitting. Thin lines denote dynamics predicted using each of the best parameter combinations identified in the final iteration of iABC (see SI.Methods). Thick lines indicates average of these simulations.

**Figure S6 Alternate model, $\mathbf{M}_2^1$: $f_{CM}$ formulation variant where $f_{CM} = 1 - e^{-(\frac{t}{\tau_F})^2}$** Fitting model to observed dynamics of (a) HCV, (b) JEV and (c) PV. Data source: [22, 31, 19] (d) Comparing distribution of parameter estimated for the three viruses: HCV (blue), JEV (orange) and PV (yellow). Here the fit and parameter estimates correspond to that estimated in the eighth iteration of iABC. In (a), (b) and (c), hollow circles and error bars correspond to data used for fitting, whereas similarly colored lines represent model fitting. Thin lines denote dynamics predicted using each of the best parameter combinations identified in the final iteration of iABC (see SI.Methods). Thick lines indicates average of these simulations.

**Figure S7 Alternate model, $\mathbf{M}_4^{10}$: formulation assumes that 10 $P_{NS}$ molecules are required to form one $RC_{CM}$.** Eq. 2.2 is modified to $\frac{dP_{NS}}{dt} = k_t.R_{cyt} - \mu_P.P_{NS} - 10.k_c.P_{NS}.R_{cyt}.(f_{CM} - \frac{RC_{CM}}{N_C})$. Fitting model to observed dynamics of (a) HCV, (b) JEV and (c) PV. Data source: [22, 31, 19] (d) Comparing distribution of parameter estimated for the three viruses: HCV (blue), JEV (orange) and PV (yellow). Here the fit and parameter estimates correspond to that estimated in the eighth iteration of iABC. In (a), (b) and (c), hollow circles and error bars correspond to data used for fitting, whereas

similarly colored lines represent model fitting. Thin lines denote dynamics predicted using each of the best parameter combinations identified in the final iteration of iABC (see SI.Methods). Thick lines indicates average of these simulations.

**Figure S8 Alternate model, $W_4$: Packaging formulation variant where genomes from compartments associate with SP from cytoplasm to form new viral particles** Fitting model to observed dynamics of (a) HCV, (b) JEV and (c) PV. Data source: [22, 31, 19] (d) Comparing distribution of parameter estimated for the three viruses: HCV (blue), JEV (orange) and PV (yellow). Here the fit and parameter estimates correspond to that estimated in the eighth iteration of iABC. In (a), (b) and (c), hollow circles and error bars correspond to data used for fitting, whereas similarly colored lines represent model fitting. Thin lines denote dynamics predicted using each of the best parameter combinations identified in the final iteration of iABC (see SI.Methods). Thick lines indicates average of these simulations.

**Figure S9 Parameter-temporal sensitivity profiles level of viral (+)RNA in cytoplasm ($R_{cyt}$)** for HCV [left], JEV [center] and PV [right], for MOI 3. Here $S(X)$ denote the profile associated with parameter, X, and $S_R = S(\mu_P) + S(\mu_V) + S(dummy)$. Time axis is not to scale across profiles for different viruses.

**Figure S10 Cellular infectivity profiles**: Variation of cellular infectivity, $\Phi$ with compartment formation delay ($\tau_F$) and degradation rate of viral (+)RNA in cytoplasm ($\mu_R$) for (a) HCV, (b) JEV and (c) PV evaluated for viral seeding (N) of 3. Variation of $\Phi$ with $\tau_F$ and viral translation rate ($k_t$) for (d) HCV, (e) JEV and (f) PV evaluated for viral seeding (N) of 3. Color scale may vary across the sub-figures.

**Figure S11 Influence of $\Phi$ on early life cycle parameters is dependent on Viral seeding (N) and virus-host system:** Fold change in $\Phi$ for (a) HCV and (b) JEV with varying N for different parameters. $k_t^{WT}$, $k_c^{WT}$ and $\tau_F^{WT}$ denotes the median value of parameter for the corresponding (Table 1), and $\mu_R^{WT} = 0.25$ h$^{-1}$.

**Figure S12 Synergestic strategies to reduce cellular infectivity:** Synergy profile $\Psi(\tau_F, \mu_R)$ as function of compartment formation delay ($\tau_F$) and degradation rate of viral (+)RNA in cytoplasm ($\mu_R$) for (a) JEV and (b) PV evaluated for viral seeding (N) of 3. Synergy profile $\Psi(\tau_F, k_t)$ as function of $\tau_F$ and viral translation rate ($k_t$) for (c) HCV, (d) JEV and (e) PV evaluated for viral seeding (N) of 3. (f) Variation of $\Psi(\tau_F, k_t)$ for different perturbation strengths (denoted by different markers) with viral seeding (N) for HCV (blue), JEV (red) and PV (yellow). (g) $\Psi(\tau_F, k_t)$ shows a negative correlation with $\{(1-p_0)+p_{12}\}$, which increases as it approaches either the limit of 'deterministic sustenance ($p_{12} \to 1$)'

or 'deterministic extinction ($p_0 \to 0$)'. Here $\tau_F^{WT}$ and $k_t^{WT}$ corresponds to corresponding estimate for the virus and $\mu_R^{WT} = 0.25$ h$^{-1}$. Color scale may vary across the sub-figures (a-e). Marker properties are consistent in (f) and (g) and larger markers correspond to higher N.

**Table S1 Compartment formation dynamics: Parameter estimation and goodness of fit**

**Table S2 Cellular life cycle model: Parameter estimation summary**

**Table S3 Comparing parameter estimation for sgHCV (JFH1 strain) life cycle in host cells of different permissivity**

**Table S4 Comparing parameter estimation and goodness of fit for model variants**

**Table S5 Interventions to perturb parameters**

# References


[1] Sven Miller and Jacomine Krijnse-Locker. Modification of intracellular membrane structures for virus replication. *Nature Reviews Microbiology*, 6(5):363–374, 2008.

[2] Johan A den Boon and Paul Ahlquist. Organelle-like membrane compartmentalization of positive-strand rna virus replication factories. *Annual review of microbiology*, 64:241–256, 2010.

[3] David Paul and Ralf Bartenschlager. Architecture and biogenesis of plus-strand rna virus replication factories. *World journal of virology*, 2(2):32, 2013.

[4] Inés Romero-Brey and Ralf Bartenschlager. Membranous replication factories induced by plus-strand rna viruses. *Viruses*, 6(7):2826–2857, 2014.

[5] Ming-Jhan Wu, Po-Yuan Ke, John T-A Hsu, Chau-Ting Yeh, and Jim-Tong Horng. Reticulon 3 interacts with ns4b of the hepatitis c virus and negatively regulates viral replication by disrupting ns4b self-interaction. *Cellular microbiology*, 16(11):1603–1618, 2014.

[6] Wen-Fang Tang, Shing-Ying Yang, Bin-Wen Wu, Jia-Rong Jheng, Yin-Li Chen, Chung-Hsuan Shih, Kwang-Huei Lin, Hsin-Chi Lai, Petrus Tang, and Jim-Tong Horng. Reticulon 3 binds the 2c protein of enterovirus 71 and is required for viral replication. *Journal of Biological Chemistry*, 282(8):5888–5898, 2007.

[7] Turgut E Aktepe, Susann Liebscher, Julia E Prier, Cameron P Simmons, and Jason M Mackenzie. The host protein reticulon 3.1 a is utilized by flaviviruses to facilitate membrane remodelling. *Cell reports*, 21(6):1639–1654, 2017.

[8] Anna Lundin, Ronald Dijkman, Tomas Bergström, Nina Kann, Beata Adamiak, Charles Hannoun, Eveline Kindler, Hulda R Jonsdottir, Doreen Muth, Joeri Kint, et al. Targeting membrane-bound viral rna synthesis reveals potent inhibition of diverse coronaviruses including the middle east respiratory syndrome virus. *PLoS pathogens*, 10(5), 2014.

[9] Obdulio García-Nicolás, Philip V'kovski, Nathalie J Vielle, Nadine Ebert, Roland Züst, Jasmine Portmann, Hanspeter Stalder, Véronique Gaschen, Gabrielle Vieyres, Michael Stoffel, et al. The small-compound inhibitor k22 displays broad antiviral activity against different members of the family flaviviridae and offers potential as a panviral inhibitor. *Antimicrobial agents and chemotherapy*, 62(11):e01206–18, 2018.

[10] Carola Berger, Inés Romero-Brey, Danijela Radujkovic, Raphael Terreux, Margarita Zayas, David Paul, Christian Harak, Simone Hoppe, Min Gao, Francois Penin, et al. Daclatasvir-like inhibitors of ns5a block early biogenesis of hepatitis c virus–induced membranous replication factories, independent of rna replication. *Gastroenterology*, 147(5):1094–1105, 2014.

[11] Kristi L Berger, Sean M Kelly, Tristan X Jordan, Michael A Tartell, and Glenn Randall. Hepatitis c virus stimulates the phosphatidylinositol 4-kinase iii alpha-dependent phosphatidylinositol 4-phosphate production that is essential for its replication. *Journal of virology*, 85(17):8870–8883, 2011.

[12] Michael B Schulte and Raul Andino. Single-cell analysis uncovers extensive biological noise in poliovirus replication. *Journal of virology*, 88(11):6205–6212, 2014.

[13] Frank S Heldt, Sascha Y Kupke, Sebastian Dorl, Udo Reichl, and Timo Frensing. Single-cell analysis and stochastic modelling unveil large cell-to-cell variability in influenza a virus infection. *Nature communications*, 6(1):1–12, 2015.

[14] Ranjan Srivastava, L You, J Summers, and J Yin. Stochastic vs. deterministic modeling of intracellular viral kinetics. *Journal of theoretical biology*, 218(3):309–321, 2002.

[15] Berend Snijder, Raphael Sacher, Pauli Rämö, Eva-Maria Damm, Prisca Liberali, and Lucas Pelkmans. Population context determines cell-to-cell variability in endocytosis and virus infection. *Nature*, 461(7263):520–523, 2009.

[16] Harel Dahari, Ruy M Ribeiro, Charles M Rice, and Alan S Perelson. Mathematical modeling of subgenomic hepatitis c virus replication in huh-7 cells. *Journal of virology*, 81(2):750–760, 2007.

[17] Marco Binder, Nurgazy Sulaimanov, Diana Clausznitzer, Manuel Schulze, Christian M Hüber, Simon M Lenz, Johannes P Schlöder, Martin Trippler, Ralf Bartenschlager, Volker Lohmann, et al. Replication vesicles are load-and choke-points in the hepatitis c virus lifecycle. *PLoS pathogens*, 9(8), 2013.

[18] Roland R Regoes, Shane Crotty, Rustom Antia, and Mark M Tanaka. Optimal replication of poliovirus within cells. *The American Naturalist*, 165(3):364–373, 2005.

[19] Michael B Schulte, Jeremy A Draghi, Joshua B Plotkin, and Raul Andino. Experimentally guided models reveal replication principles that shape the mutation distribution of rna viruses. *Elife*, 4:e03753, 2015.

[20] Alison K McLean, Fabio Luciani, and Mark M Tanaka. Trade-offs in resource allocation in the intracellular life-cycle of hepatitis c virus. *Journal of theoretical biology*, 267(4):565–572, 2010.

[21] Diana Clausznitzer, Julia Harnisch, and Lars Kaderali. Multi-scale model for hepatitis c viral load kinetics under treatment with direct acting antivirals. *Virus research*, 218:96–101, 2016.

[22] Thomas R Aunins, Katherine A Marsh, Gitanjali Subramanya, Susan L Uprichard, Alan S Perelson, and Anushree Chatterjee. Intracellular hepatitis c virus modeling predicts infection dynamics and viral protein mechanisms. *Journal of virology*, 92(11):e02098–17, 2018.

[23] Carolin Zitzmann, Bianca Schmid, Alessia Ruggieri, Alan S Perelson, Marco Binder, Ralf Bartenschlager, and Lars Kaderali. A coupled mathematical model of the intracellular replication of dengue virus and the host cell immune response to infection. *Frontiers in microbiology*, 11:725, 2020.

[24] Ashley I Teufel, Wu Liu, Jeremy A Draghi, Craig E Cameron, and Claus O Wilke. Uncovering modeling features of viral replication dynamics from high-throughput single-cell virology experiments. *bioRxiv*, 2020.

[25] John Yin and Jacob Redovich. Kinetic modeling of virus growth in cells. *Microbiology and Molecular Biology Reviews*, 82(2), 2018.

[26] Carolin Zitzmann and Lars Kaderali. Mathematical analysis of viral replication dynamics and antiviral treatment strategies: from basic models to age-based multi-scale modeling. *Frontiers in microbiology*, 9:1546, 2018.

[27] Alan S Perelson, Eva Herrmann, Florence Micol, and Stefan Zeuzem. New kinetic models for the hepatitis c virus. *Hepatology*, 42(4):749–754, 2005.

[28] THT Nguyen and J Guedj. Hcv kinetic models and their implications in drug development. *CPT: pharmacometrics & systems pharmacology*, 4(4):231–242, 2015.

[29] Anat Zimmer, Itay Katzir, Erez Dekel, Avraham E Mayo, and Uri Alon. Prediction of multidimensional drug dose responses based on measurements of drug pairs. *Proceedings of the National Academy of Sciences*, 113(37):10442–10447, 2016.

[30] P Padmanabhan and NM Dixit. Modeling suggests a mechanism of synergy between hepatitis c virus entry inhibitors and drugs of other classes. *CPT: pharmacometrics & systems pharmacology*, 4(8):445–453, 2015.

[31] Pradeep Devappa Uchil and Vijaya Satchidanandam. Characterization of rna synthesis, replication mechanism, and in vitro rna-dependent rna polymerase activity of japanese encephalitis virus. *Virology*, 307(2):358–371, 2003.

[32] Ronald WAL Limpens, Hilde M van der Schaar, Darshan Kumar, Abraham J Koster, Eric J Snijder, Frank JM van Kuppeveld, and Montserrat Bárcena. The transformation of enterovirus replication structures: a three-dimensional study of single-and double-membrane compartments. *MBio*, 2(5):e00166–11, 2011.

[33] Barbara van der Hoeven, Diede Oudshoorn, Abraham J Koster, Eric J Snijder, Marjolein Kikkert, and Montserrat Bárcena. Biogenesis and architecture of arterivirus replication organelles. *Virus research*, 220:70–90, 2016.

[34] David Paul, Inés Romero-Brey, Jérôme Gouttenoire, Savina Stoitsova, Jacomine Krijnse-Locker, Darius Moradpour, and Ralf Bartenschlager. Ns4b self-interaction through conserved c-terminal elements is required for the establishment of functional hepatitis c virus replication complexes. *Journal of virology*, 85(14):6963–6976, 2011.

[35] Terence L Wagner, Hsin-I Wu, Peter JH Sharpe, and RN Coulson. Modeling distributions of insect development time: a literature review and application of the weibull function. *Annals of the Entomological Society of America*, 77(5):475–483, 1984.

[36] Kèvin Knoops, Montserrat Bárcena, Ronald WAL Limpens, Abraham J Koster, A Mieke Mommaas, and Eric J Snijder. Ultrastructural characterization of arterivirus replication structures: reshaping the endoplasmic reticulum to accommodate viral rna synthesis. *Journal of virology*, 86(5):2474–2487, 2012.

[37] Mustafa Ulasli, Monique H Verheije, Cornelis AM de Haan, and Fulvio Reggiori. Qualitative and quantitative ultrastructural analysis of the membrane rearrangements induced by coronavirus. *Cellular microbiology*, 12(6):844–861, 2010.

[38] Inés Romero-Brey, Andreas Merz, Abhilash Chiramel, Ji-Young Lee, Petr Chlanda, Uta Haselman, Rachel Santarella-Mellwig, Anja Habermann, Simone Hoppe, Stephanie Kallis, et al. Three-dimensional architecture and biogenesis of membrane structures associated with hepatitis c virus replication. *PLoS pathogens*, 8(12), 2012.

[39] Mirko Cortese, Sarah Goellner, Eliana Gisela Acosta, Christopher John Neufeldt, Olga Oleksiuk, Marko Lampe, Uta Haselmann, Charlotta Funaya, Nicole Schieber, Paolo Ronchi, et al. Ultrastructural characterization of zika virus replication factories. *Cell reports*, 18(9):2113–2123, 2017.

[40] Boerries Brandenburg, Lily Y Lee, Melike Lakadamyali, Michael J Rust, Xiaowei Zhuang, and James M Hogle. Imaging poliovirus entry in live cells. *PLoS Biol*, 5(7):e183, 2007.

[41] Jong-Won Oh, Takayoshi Ito, and Michael MC Lai. A recombinant hepatitis c virus rna-dependent rna polymerase capable of copying the full-length viral rna. *Journal of Virology*, 73(9):7694–7702, 1999.

[42] Graham R Cleaves, Terence E Ryan, and R Walter Schlesinger. Identification and characterization of type 2 dengue virus replicative intermediate and replicative form rnas. *Virology*, 111(1):73–83, 1981.

[43] Hongliang Wang and Andrew W Tai. Continuous de novo generation of spatially segregated hepatitis c virus replication organelles revealed by pulse-chase imaging. *Journal of hepatology*, 66(1):55–66, 2017.

[44] Oliver Grünvogel, Ombretta Colasanti, Ji-Young Lee, Volker Klöss, Sandrine Belouzard, Anna Reustle, Katharina Esser-Nobis, Jasper Hesebeck-Brinckmann, Pascal Mutz, Katrin Hoffmann, et al. Secretion of hepatitis c virus replication intermediates reduces activation of toll-like receptor 3 in hepatocytes. *Gastroenterology*, 154(8):2237–2251, 2018.

[45] Chunfu Wang, Jill Pflugheber, Rhea Sumpter, Donald L Sodora, Daniel Hui, Ganes C Sen, and Michael Gale. Alpha interferon induces distinct translational control programs to suppress hepatitis c virus rna replication. *Journal of virology*, 77(7):3898–3912, 2003.

[46] Margaret Robinson, Huiling Yang, Siu-Chi Sun, Betty Peng, Yang Tian, Nikos Pagratis, Andrew E Greenstein, and William E Delaney. Novel hepatitis c virus reporter replicon cell lines enable efficient antiviral screening against genotype 1a. *Antimicrobial agents and chemotherapy*, 54(8):3099–3106, 2010.

[47] Jamie J Arnold and Craig E Cameron. Poliovirus rna-dependent rna polymerase (3dpol) assembly of stable, elongation-competent complexes by using a symmetrical primer-template substrate (sym/sub). *Journal of Biological Chemistry*, 275(8):5329–5336, 2000.

[48] David Baltimore. Structure of the poliovirus replicative intermediate rna. *Journal of molecular biology*, 32(2):359–368, 1968.

[49] Oliver C Richards, Susan C Martin, Holly G Jense, and Ellie Ehrenfeld. Structure of poliovirus replicative intermediate rna: electron microscope analysis of rna cross-linked in vivo with psoralen derivative. *Journal of molecular biology*, 173(3):325–340, 1984.

[50] Lihui Liu, Hongping Dong, Hui Chen, Jing Zhang, Hua Ling, Zhong Li, Pei-Yong Shi, and Hongmin Li. Flavivirus rna cap methyltransferase: structure, function, and inhibition. *Frontiers in biology*, 5(4):286–303, 2010.

[51] Graham R Cleaves and Donald T Dubin. Methylation status of intracellular dengue type 2 40 s rna. *Virology*, 96(1):159–165, 1979.

[52] Richard J Kuhn, Wei Zhang, Michael G Rossmann, Sergei V Pletnev, Jeroen Corver, Edith Lenches, Christopher T Jones, Suchetana Mukhopadhyay, Paul R Chipman, Ellen G Strauss, et al. Structure of dengue virus: implications for flavivirus organization, maturation, and fusion. *Cell*, 108(5):717–725, 2002.

[53] Christian G Schüttler, Christine Thomas, Thomas Discher, Georg Friese, Jürgen Lohmeyer, Ralph Schuster, Stephan Schaefer, and Wolfram H Gerlich. Variable ratio of hepatitis c virus rna to viral core antigen in patient sera. *Journal of clinical microbiology*, 42(5):1977–1981, 2004.

[54] Jing-Yi Lin, Tzu-Chun Chen, Kuo-Feng Weng, Shih-Cheng Chang, Li-Lien Chen, and Shin-Ru Shih. Viral and host proteins involved in picornavirus life cycle. *Journal of biomedical science*, 16(1):103, 2009.

[55] Sun Ju Keum, Sung Mi Park, Ji Hoon Park, Jong Ha Jung, Eun Ji Shin, and Sung Key Jang. The specific infectivity of hepatitis c virus changes through its life cycle. *Virology*, 433(2):462–470, 2012.

[56] Nikita V Ivanisenko, Elena L Mishchenko, Ilya R Akberdin, Pavel S Demenkov, Vitaly A Likhoshvai, Konstantin N Kozlov, Dmitry I Todorov, Vitaly V Gursky, Maria G Samsonova, Alexander M Samsonov, et al. A new stochastic model for subgenomic hepatitis c virus replication considers drug resistant mutants. *PloS one*, 9(3):e91502, 2014.

[57] Simeone Marino, Ian B Hogue, Christian J Ray, and Denise E Kirschner. A methodology for performing global uncertainty and sensitivity analysis in systems biology. *Journal of theoretical biology*, 254(1):178–196, 2008.

[58] Jérôme Gouttenoire, Philippe Roingeard, François Penin, and Darius Moradpour. Amphipathic $\alpha$-helix ah2 is a major determinant for the oligomerization of hepatitis c virus nonstructural protein 4b. *Journal of virology*, 84(24):12529–12537, 2010.

[59] Arturo Diaz, Xiaofeng Wang, and Paul Ahlquist. Membrane-shaping host reticulon proteins play crucial roles in viral rna replication compartment formation and function. *Proceedings of the National Academy of Sciences*, 107(37):16291–16296, 2010.

[60] Arturo Diaz and Paul Ahlquist. Role of host reticulon proteins in rearranging membranes for positive-strand rna virus replication. *Current opinion in microbiology*, 15(4):519–524, 2012.

[61] Kristi L Berger, Jacob D Cooper, Nicholas S Heaton, Rosa Yoon, Todd E Oakland, Tristan X Jordan, Guaniri Mateu, Arash Grakoui, and Glenn Randall. Roles for endocytic trafficking and phosphatidylinositol 4-kinase iii alpha in hepatitis c virus replication. *Proceedings of the National Academy of Sciences*, 106(18):7577–7582, 2009.

[62] Kristi L Berger and Glenn Randall. Potential roles for cellular cofactors in hepatitis c virus replication complex formation. *Communicative & integrative biology*, 2(6):471–473, 2009.

[63] Minetaro Arita, Hirotatsu Kojima, Tetsuo Nagano, Takayoshi Okabe, Takaji Wakita, and Hiroyuki Shimizu. Phosphatidylinositol 4-kinase iii beta is a target of enviroxime-like compounds for antipoliovirus activity. *Journal of virology*, 85(5):2364–2372, 2011.

[64] Haihong Zhu, Flossie Wong-Staal, Haekyung Lee, Andrew Syder, Jeffrey McKelvy, Robert T Schooley, and David L Wyles. Evaluation of itx 5061, a scavenger receptor b1 antagonist: resistance selection and activity in combination with other hepatitis c virus antivirals. *Journal of Infectious Diseases*, 205(4):656–662, 2012.

[65] Fei Xiao, Isabel Fofana, Christine Thumann, Laurent Mailly, Roxane Alles, Eric Robinet, Nicolas Meyer, Mickaël Schaeffer, François Habersetzer, Michel Doffoël, et al. Synergy of entry inhibitors with direct-acting antivirals uncovers novel combinations for prevention and treatment of hepatitis c. *Gut*, 64(3):483–494, 2015.

[66] CI Bliss. The toxicity of poisons applied jointly 1. *Annals of applied biology*, 26(3):585–615, 1939.

[67] Mauricio Comas-Garcia. Packaging of genomic rna in positive-sense single-stranded rna viruses: A complex story. *Viruses*, 11(3):253, 2019.

[68] Yutong Song, Oleksandr Gorbatsevych, Ying Liu, JoAnn Mugavero, Sam H Shen, Charles B Ward, Emmanuel Asare, Ping Jiang, Aniko V Paul, Steffen Mueller, et al. Limits of variation, specific infectivity, and genome packaging of massively recoded poliovirus genomes. *Proceedings of the National Academy of Sciences*, 114(41):E8731–E8740, 2017.

[69] Elizabeth R Aguilera, Andrea K Erickson, Palmy R Jesudhasan, Christopher M Robinson, and Julie K Pfeiffer. Plaques formed by mutagenized viral populations have elevated coinfection frequencies. *MBio*, 8(2), 2017.

[70] Volker Lohmann, Sandra Hoffmann, Ulrike Herian, Francois Penin, and Ralf Bartenschlager. Viral and cellular determinants of hepatitis c virus rna replication in cell culture. *Journal of virology*, 77(5):3007–3019, 2003.

[71] Keril J Blight, Jane A McKeating, and Charles M Rice. Highly permissive cell lines for subgenomic and genomic hepatitis c virus rna replication. *Journal of virology*, 76(24):13001–13014, 2002.

[72] Mark A Beaumont, Wenyang Zhang, and David J Balding. Approximate bayesian computation in population genetics. *Genetics*, 162(4):2025–2035, 2002.

[73] Andrea Saltelli and Ricardo Bolado. An alternative way to compute fourier amplitude sensitivity test (fast). *Computational Statistics & Data Analysis*, 26(4):445–460, 1998.

[74] Daniel T Gillespie. Exact stochastic simulation of coupled chemical reactions. *The journal of physical chemistry*, 81(25):2340–2361, 1977.